

Thermally fixed reflection gratings for infrared light in LiNbO₃:Ti:Fe channel waveguides

J. Hukriede, I. Nee, D. Kip, and E. Krätzig

Fachbereich Physik, Universität Osnabrück, D-49069 Osnabrück, Germany

Received March 20, 1998

We present a narrow-bandwidth interference filter in an optical monomode LiNbO₃:Ti:Fe channel waveguide operating in the infrared wavelength region around $\lambda = 1.55 \mu\text{m}$. The filter consists of a thermally fixed refractive-index Bragg grating recorded with visible green light by use of a holographic technique. In a first approach we measure a reflectivity for the infrared light of 60% and a linewidth (FWHM) of 0.11 nm. © 1998 Optical Society of America

OCIS codes: 090.0090, 130.0130, 260.3060, 160.3730, 230.1480, 230.7380.

Thermally fixed refractive-index gratings in LiNbO₃:Fe crystals operating in the infrared wavelength region near $\lambda = 1.55 \mu\text{m}$ are of interest in integrated optics. Recently a LiNbO₃:Ti:Fe:Er distributed Bragg reflection waveguide laser¹ with a fixed reflection grating was designed and investigated. Other applications can be found in the field of optical data transmission and signal processing: For example, the capacity of present fiber networks is enhanced by wavelength-division multiplexing, which can be done by superimposition of precisely oriented fixed holographic gratings in a LiNbO₃ sample. Furthermore, highly spectrum-selective filters working with counterpropagating beams are under development and were recently demonstrated in bulk crystals.^{2,3} Nevertheless, if such a device is used in conjunction with fiber and integrated optics, waveguide structures are of considerable importance. Following this idea, in this Letter a narrow-bandwidth spectral filter for infrared light is presented and investigated in a photorefractive LiNbO₃:Ti:Fe channel waveguide.

Titanium strips were fabricated on our *y*-cut LiNbO₃ samples along the *c* axis. The refractive-index profile $n(x, y)$ after indiffusion was determined with the help of diffusion theory.⁴ A Gauss-Hermite-Gauss (GHG) approximation technique⁵ was used to describe the field distribution of the TE₀ and TM₀ modes in the channel waveguides: By solution of the Helmholtz equation the effective refractive index n_{eff} could be derived. The effective refractive index of the first excited modes TE₁ and TM₁ was obtained in a similar way by use of a HGHG approximation.

First we used the GHG formalism to optimize the diffusion time and the titanium-layer thickness for a 6- μm -wide monomode channel waveguide operating at a wavelength of $\lambda = 1559.00 \text{ nm}$. In this way the titanium concentration was kept at a low level: In previous experiments with planar multimode guides⁶ it turned out that thermal fixing worked best deep in the waveguide layer in which the titanium concentration was lowest.

An undoped LiNbO₃ wafer of congruently melting composition was cut into pieces measuring 7 mm ×

1 mm × 16 mm, with the *c* axis pointing along the largest dimension. Then the samples were coated with iron layers of various thicknesses. Here we present data for a thickness of the iron layer $\tau_{\text{Fe}} = 10 \text{ nm}$, which we indiffused at a temperature of 1030 °C in air to increase the impurity level and thus the photorefractive effect. The diffusion time was 96 h, long enough to ensure an almost constant iron concentration over the waveguide region. In a second step a 100-nm-thick layer of titanium was deposited, and with a photolithographic technique a set of thin strips of different width *W* was produced on the crystal. These channels were indiffused for 18 h in air at a temperature of 1000 °C. Then a short reducing treatment of 2 h in an argon atmosphere at 1025 °C was applied. Here we pumped the argon gas through water to increase the proton concentration of the samples, which is important for an efficient thermal fixing process.⁷ The proton concentration was determined by absorption measurements along the *y* axis with a Fourier spectrometer.⁸ We obtained $c_{\text{H}^+} = 5.6 \times 10^{24} \text{ m}^{-3}$.

We fabricated the filter by recording a refractive-index grating in the sample with a two-beam holographic setup. Two coherent ordinarily polarized light beams of an argon-ion laser at a wavelength of $\lambda_w = 514.5 \text{ nm}$ were expanded to a $1/e^2$ diameter of ~20 mm. The beams impinged symmetrically upon the top face of the sample in the *yz* plane, intersecting at an angle 2Θ in air. The writing angle could be adjusted with an accuracy better than 0.02°. Each beam had an intensity of 580 W m⁻². In photorefractive LiNbO₃, illumination with a sinusoidal interference pattern leads to the formation of a refractive-index grating. Here the grating period was $\Lambda = \lambda_w / (2 \sin \Theta)$. The thermal fixing procedure was performed in the following way: First the waveguide was heated to a constant temperature of 180 °C. Then the two beams were switched on and the grating was recorded by use of an active stabilization system.⁶ Protons became mobile and compensated for the generated space-charge field. After recording the sample was cooled to room temperature within 5 min. The fixed hologram was developed by illuminating the whole sample homogeneously with a halogen lamp for

30 min. Modulated photocurrents originating from a modulated distribution of filled and empty traps arose, and the fixed grating appeared.

The setup for readout in reflection geometry is illustrated in Fig. 1. A distributed feedback laser tunable in steps of 0.01 nm served as the infrared light source. The output beam was connected to a nonpolarizing fiber with a graded-index collimator at its end. A polarizer allowed us to excite either the TE_0 or the TM_0 mode. The beam was coupled into the channel via a $25\times$ microscope lens and was imaged upon photodetector 1 via a $10\times$ microscope lens. A small iris diaphragm rejected stray light. The light diffracted from the grating impinged upon photodetector 2. During readout the wavelength of the laser was tuned, and the signal of the two detectors was stored by a computer for identification of the peak wavelength λ_p , which depends on the period Λ through the relation $\Lambda = \lambda_p / (2n_{\text{eff}})$.

Interpolation of data from Ref. 9 yielded the bulk ordinary refractive index $n_b = 2.2109$ of undoped LiNbO_3 at $\lambda_p = 1559.00$ nm. For a grating written at room temperature this resulted in a period of $\Lambda = 352.572$ nm in the substrate. The corresponding recording angle for the green light was $2\Theta = 93.71^\circ$. A GHG simulation (see above) for the TE_0 mode in a $6\text{-}\mu\text{m}$ -wide channel yielded $n_{\text{eff}} = 2.2116$. It follows that λ_p increased by 0.5 nm when the grating was read with light guided in this channel. Furthermore, the indiffused iron caused a nearly constant slight increase of the refractive index n_b in the channels,¹⁰ resulting in an additional small increase of λ_p . The thermal expansion of LiNbO_3 at 180°C must be taken into account, too.^{3,11} We roughly estimate that the peak wavelength of a grating recorded at 180°C is reduced by 1 nm when the sample is cooled down.

First a grating was fixed for 190 min in the waveguide. After developing the hologram, a TE-polarized weak light beam was coupled into the $6\text{-}\mu\text{m}$ -wide channel. Figure 2 shows the normalized transmitted and reflected beam power P versus the readout wavelength λ . A constant background resulting from Fresnel reflections has been subtracted from the reflected signal. A narrow peak appears at $\lambda_p = 1559.51$ nm, with a FWHM of 0.11 nm. From the transmitted signal a diffraction efficiency of $\eta = 60\%$ is derived. The peak positions of the diffracted and the transmitted beams do not match exactly.

In Fig. 3 the transmittance curves $P_{\text{trans}}(\lambda)$ are presented for channels with different widths W . The peak wavelength λ_p during readout increases with increasing W from 1559.51 to 1560.46 nm. On the other hand, the grating reflectance decreases with W . A second small peak in the region around $\lambda_p' = 1559.10$ nm can be observed for all channels except $W = 6, 10\ \mu\text{m}$.

We also checked the polarization dependence of the peak wavelength λ_p . In Fig. 4 the transmitted power $P_{\text{trans}}(\lambda)$ is depicted for unpolarized light as well as for polarization states TE and TM. Again, the $6\text{-}\mu\text{m}$ -wide channel was investigated. The peak position, reflectivity, and FWHM for the TE_0 mode were already mentioned above. For the TM_0 mode we

measured an efficiency of 58%, a center wavelength of $\lambda_p = 1559.47$ nm, and a FWHM of 0.12 nm. With unpolarized light the peak position is 1559.50 nm.

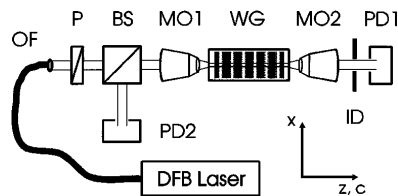


Fig. 1. Setup for readout of fixed gratings: OF, optical fiber; P, polarizer; BS, beam splitter; MO1 (MO2), $25\times$ ($10\times$) microscope lens; WG, waveguide; ID, iris diaphragm; PD1, PD2, photodetectors; DFB, distributed feedback.

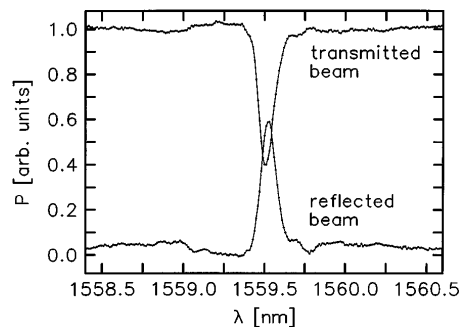


Fig. 2. Power P of the transmitted and the reflected TE-polarized beams versus readout wavelength λ for a fixed grating in the waveguide.

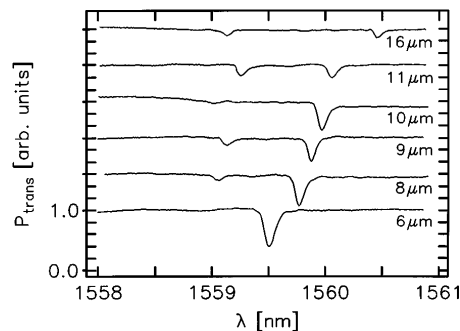


Fig. 3. Transmitted power P_{trans} versus readout wavelength λ for TE-polarized light propagating through the different channels of the waveguide.

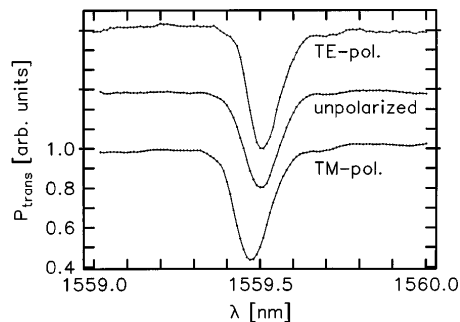


Fig. 4. Transmitted power P_{trans} versus readout wavelength λ for unpolarized light as well as for polarization states TE and TM.

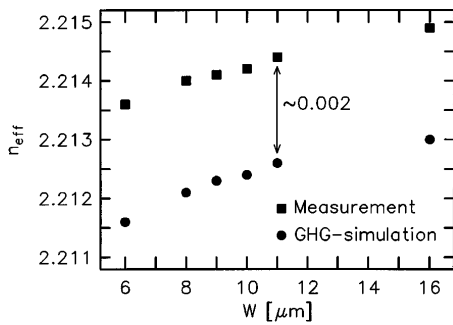


Fig. 5. Calculated and measured effective refractive indices n_{eff} versus channel width W .

The diffraction efficiency reaches 50% with a peak width of 0.12 nm.

From the measured peak values λ_p of Fig. 3 and the calculated grating period Λ the effective refractive index n_{eff} of the TE_0 mode in the various channels can be derived. To consider thermal expansion during recording we used the coefficient $\alpha_{33} \approx 5.6 \times 10^{-6} \text{ K}^{-1}$.³ The experimental data are summarized in Fig. 5 together with the calculated values obtained with the GHG formalism. For the latter values the bulk refractive index $n_b = 2.2109$ was employed. All measured n_{eff} values were ~ 0.002 higher than the calculated ones. This difference can be partly explained by an increase of the refractive index n_b that results from the indiffused iron. The effective refractive indices n_{eff} will be shifted in the same way. Lithium outdiffusion is not supposed to play a major role in the peak shift because it alters only the extraordinary refractive index of LiNbO_3 . On the other hand, one could think of a mismatch of the recording angle 2θ (see equations above), but this would require a displacement of more than $\Delta(2\theta) = 0.11^\circ$.

The appearance of the second peak even for $W \leq 10 \mu\text{m}$, where the channels are certainly monomode, can be explained in the following way: Imperfect incoupling always generates unguided stray light propagating through the sample with n_b . The light is also diffracted from the fixed grating, yielding a second peak at a smaller wavelength. If the unguided light is not completely blocked this peak will be detected, too. We are planning to overcome this problem by directly coupling an optical single-mode fiber to the end of the channel waveguide so that the diverging stray light will not be coupled in.

The application of an integrated device based on a $\text{LiNbO}_3:\text{Ti}$ channel waveguide requires that the peak values for the TE_0 and TM_0 modes nearly coincide. This requirement follows from the fact that optical fibers used in telecommunications are not polarization preserving. A GHG simulation is in good agreement with the data shown in Fig. 4. The calculated peak difference between the TE_0 and the TM_0 modes is 0.06 nm, and the experiment yields a difference of

$0.04 \pm 0.02 \text{ nm}$. The observation that the grating reflectivity for unpolarized light is less than that for the TE_0 and the TM_0 modes may result from this deviation, too. If unpolarized light is coupled into the channel both modes are excited. As a consequence of their different effective refractive indices in the $6\text{-}\mu\text{m}$ -wide channel, they cannot both be simultaneously reflected at the same readout wavelength. If one mode is reflected best, the other will still be transmitted through the grating rather well, and the peak efficiency will decrease.

The long-term stability of the device is governed by the dark conductivity, which is not negligible in the investigated waveguide: Even in the dark the developed grating is slowly compensated for by mobile charge carriers, and its peak reflectivity η decreases to its $1/e$ value within ~ 17 days. Nevertheless, a new developing process builds up the space-charge field again and restores it to its initial value. The real destruction of the fixed grating as a result of protonic mobility even at room temperature is much slower (time constants of months to probably years) and is under investigation.

In summary, we conclude that with adequate design the $\text{LiNbO}_3:\text{Ti}:\text{Fe}$ waveguide interference filter that has been described here will operate independently of polarization at a desired wavelength combining a high peak reflectivity with a very small bandwidth of 0.1 nm.

Financial support from the Deutsche Forschungsgemeinschaft (grant SFB 225, D9) is gratefully acknowledged.

References

1. C. Becker, A. Greiner, T. Oesselke, A. Pape, W. Sohler, and H. Suche, Universität-GH Paderborn, D-33098 Paderborn, Germany (personal communication, March, 1998).
2. V. Leyva, G. A. Rakuljic, and B. O'Connor, *Appl. Phys. Lett.* **65**, 1079 (1994).
3. R. Müller, J. V. Alvarez-Bravo, L. Arizmendi, and J. M. Cabrera, *J. Phys. D* **27**, 1628 (1994).
4. G. B. Hocker and W. K. Burns, *Appl. Opt.* **16**, 113 (1977).
5. S. K. Korotky, W. J. Minford, L. L. Buhl, M. D. Divino, and R. C. Alferness, *IEEE J. Quantum Electron.* **QE-18**, 1796 (1982).
6. J. Hukriede, D. Kip, and E. Krätzig, *Appl. Phys. B* **66**, 333 (1998).
7. K. Buse, S. Breer, K. Peithmann, S. Kapphann, M. Gao, and E. Krätzig, *Phys. Rev. B* **56**, 1225 (1997).
8. S. Kapphann and A. Breilkopf, *Phys. Status Solidi A* **133**, 159 (1992).
9. D. F. Nelson and R. M. Mikulyak, *J. Appl. Phys.* **45**, 3688 (1974).
10. D. Kip, B. Gather, H. Bendig, and E. Krätzig, *Phys. Status Solidi A* **139**, 241 (1993).
11. Y. S. Kim and R. T. Smith, *J. Appl. Phys.* **40**, 4637 (1969).